Journal of Photochemistry & Photobiology A: Chemistry 388 (2020) 112185

Contents lists available at ScienceDirect

Journal of Photochemistry & Photobiology A: Chemistry

journal homepage: www.elsevier.com/locate/jphotochem

Decorated titania fibers as photocatalysts for hydrogen generation and organic matter degradation

Sivuyisiwe Mapukata[a,b], Andrew S. Hainer[b], Anabel E. Lanterna[b], Juan C. Scaiano[b,*], Tebello Nyokong[a,*]

[a] Centre for Nanotechnology Innovation, Department of Chemistry, Rhodes University, Grahamstown, 6140, South Africa
[b] Department of Chemistry and Biomolecular Sciences and Centre for Advanced Materials Research (CAMaR), University of Ottawa, Ottawa, Ontario, K1N 6N5, Canada

ARTICLE INFO

Keywords:
Photocatalysis
Phthalocyanine photolysis
Titanium dioxide
Green chemistry
Metal nanoparticles

ABSTRACT

Heterogenous photocatalysts based on electrospun fibers composed of polyvinylpyrrolidone and titanium propoxide were prepared and heated at 500, 750 and 950 °C to obtain anatase and rutile fibers. The fibers were then decorated with Pd and Co nanoparticles as well as a symmetrical zinc phthalocyanine (Pc). The fibrous materials obtained have a paper-like macroscopic appearance allowing for easy handling and separation. The photocatalytic activities of the new materials were evaluated for the generation of H_2 upon UV (368 nm) or visible (630 nm) light excitation. Depending on the heat treatment or the post-synthetic decoration method, the materials show higher, or similar, activity compared to P25-TiO_2, with superior ease of separation. The catalysts showed ability to degrade organic matter, with MeOH used as a model compound. This is of considerable importance for potential water treatment applications that will require flow-compatible materials.

1. Introduction

Increased water pollution and the need for a cleaner environment have resulted in increased interest in heterogenous photocatalysis [1]. According to a 2017 report from the World Health Organization (WHO), over 2 billion people do not have access to safe water in their homes [2]. The degradation of water pollutants while simultaneously producing H_2 is an area of interest, mainly because H_2 has been identified as potential candidate in energy production, for example by powering fuel cells [3]. Solar water splitting to produce H_2 mediated by catalysts such as TiO_2 has risen interest since the 1972 landmark report by Fuhishima and Honda [4]. TiO_2 is particularly attractive because it has a high resistance to corrosion, possesses strong oxidising ability and it is a low-cost material [5–7]. Typical titania catalysts, including many materials described as fibers or wires at the microscopic scale, are macroscopically powders. However, for practical applications in flow systems, the separation of fine-powdered TiO_2 is difficult, making retrieval and reusability challenging. Hence, the TiO_2 fibers utilized in this work could greatly facilitate scale-up by enabling the use of flow photochemistry techniques. The TiO_2-based fibers are obtained by electrospinning followed by thermal treatment, and are easy to separate from solution. Electrospinning is a commonly used fiber fabrication technique for the production of small diameter fibers with high surface-to-volume ratio [8,9]. The TiO_2-based fibers can be prepared in different crystalline phases, i.e., anatase and rutile, enabling for comparison of their activities [10–12]. Furthermore, the fibers utilised here (in spite of their nanometric diameter) have a macroscopic thin-paper-like appearance –which remains intact even post modification– that enormously facilitates their separation and/or future potential in flow system applications (Fig. 1).

True water splitting entails breaking down water to form hydrogen and oxygen in the presence of a catalyst, such as TiO_2 (Scheme 1**A**). Unfortunately, this process is rather inefficient [13,14]. Sacrificial electron donors (SEDs) are commonly used to assist the H_2 generation thereby improving the efficiency of H_2 generation at the expense of the consumption of SEDs (Scheme 1**B**). A range of SEDs have been reported to be effective for this process [14,15], in this work 1% methanol is used as a SED. Upon exposure to UVA irradiation, an electron-hole pair is formed in the TiO_2 and methanol can quench the electrophilic hole producing $^{\bullet}CH_2OH$ radicals (Scheme 1**B**), subsequently forming formaldehyde (CH_2O) [16]. This process enhances the H_2 generation of TiO_2 by close to two orders of magnitude [14]. This phenomenon therefore suggests that other electron donor compounds, such as common organic water pollutants, can fulfil the role of being a SED and aid in effective generation of H_2 while simultaneously being degraded in the process, resulting in improved water quality [14,17].

* Corresponding authors.
E-mail addresses: titoscaiano@mac.com (J.C. Scaiano), t.nyokong@ru.ac.za (T. Nyokong).

https://doi.org/10.1016/j.jphotochem.2019.112185
Received 24 August 2019; Received in revised form 16 October 2019; Accepted 20 October 2019
Available online 24 October 2019

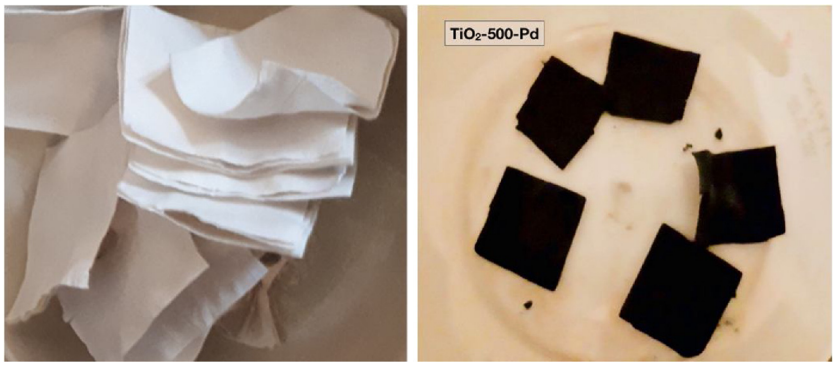

Fig. 1. Macroscopic appearance of the TiO_2 fibers (using bare (*left*) and Pd-decorated (*right*) TiO_2 fibers as examples) showing their paper-thin appearance and the change in color upon post-synthetic Pd decoration.

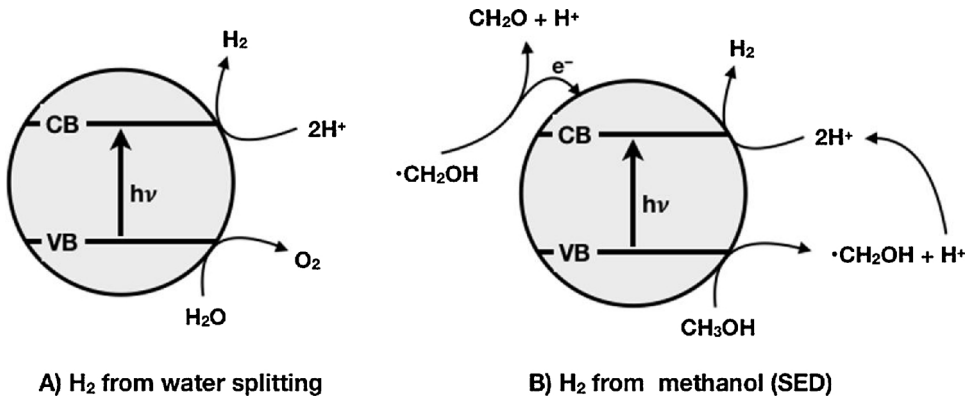

Scheme 1. (A) True water splitting versus (B) SED assisted hydrogen generation.

The generation of hydrogen as utilized here serves as an excellent way to test for new catalyst activity, as under anaerobic conditions H_2 generation is directly linked to the degradation of organic matter [17]. This work explores the use of bare, phthalocyanine (Pc) decorated and metal nanoparticle (MNP) decorated TiO_2 fibers for H_2 generation using 1% methanol as a model SED. Palladium and cobalt NPs were chosen as their efficiency in hydrogen generation when used together with commercially available P25-TiO_2 has been established before [14]. In order to compare the activities and selectivities of the TiO_2-based catalysts, their photocatalysis was conducted under 368 and 630 nm LED irradiation. The rationale behind the choices in the light sources is based on the fact that all the catalysts have TiO_2 as a dominant absorber in the UV region, and that the decoration of the fibers can change the optical properties of the materials, i.e., post-synthetic decoration provides visible light absorption properties to the material. Thus, decoration of the TiO_2 fibers with Pcs yields TiO_2 fibers with two absorbers wherein the Pc absorbs visible light. This is beneficial as most of the solar irradiation is in the visible region, making such work feasible for real life applications.

Pcs are synthetic tetrapyrrolic macrocycles containing four iminoisoindoline rings, they possess excellent visible/near infrared absorption, high thermal and chemical stability, and the ability of generate singlet oxygen [18,19]. These properties make them good candidates for applications such as dye sensitised solar cells (DSSCs), photodynamic therapy (PDT) of cancer, and photodynamic antimicrobial chemotherapy (PACT) of bacteria [20–23]. In addition, phthalocyanines have been shown to generate H_2, when adsorbed on semiconductor photocatalysts such as TiO_2, although not showing the ease of separation and flow-compatibility of the materials reported here [15,24]. In this work a symmetrical zinc Pc (complex 1, Fig. S1) is deposited on TiO_2 fibers to adapt the materials for H_2 generation and potential water treatment under flow conditions. Complex 1 was chosen because it is insoluble in water, preventing further pollution of the treated water through potential leaching mechanisms.

2. Experimental

2.1. Materials

Polyvinylpyrrolidone (PVP, MW 1,300,000), titanium(IV) propoxide (TP), 1,3-diphenylisobenzofuran (DPBF), zinc acetate ($Zn(OAc)_2$), cobalt nitrate hexahydrate, Zn phthalocyanine (ZnPc) were purchased from Sigma-Aldrich. Glacial acetic acid (AA) was purchased from Minema chemicals. Palladium (II) chloride (99%) was purchased from Alfa Aesar. Irgacure-907 (2-methyl-4′-(methylthio)-2-morpholinopropiophenone) was a gift from Ciba Specialty Chemicals. The solvents were obtained from commercial suppliers and used as received. The synthesis of complex **1** has been reported before [25,26]. Employed equipment and instrumentation are presented in the supporting information.

2.2. Electrospinning method

Sample preparation and electrospinning were conducted as reported before [27–30] with slight modifications. A solution of glacial acetic acid (5 mL) and titanium(IV) propoxide (5 mL) was prepared and added to a solution of 10 % PVP (10 mL) in ethanol. The resulting solution was stirred for 24 h and then loaded into a syringe equipped with a stainless steel needle, connected to a high voltage power supply. A voltage of 12.5 kV was applied between the needle and the stationary aluminium foil collector. The distance between the tip of the needle and the collector (TCD) was 12 cm and the applied flow rate was 1.5 mL/h (controlled using a syringe pump). The recorded temperature and humidity in the room in which the electrospinning was conducted were 24.7 °C

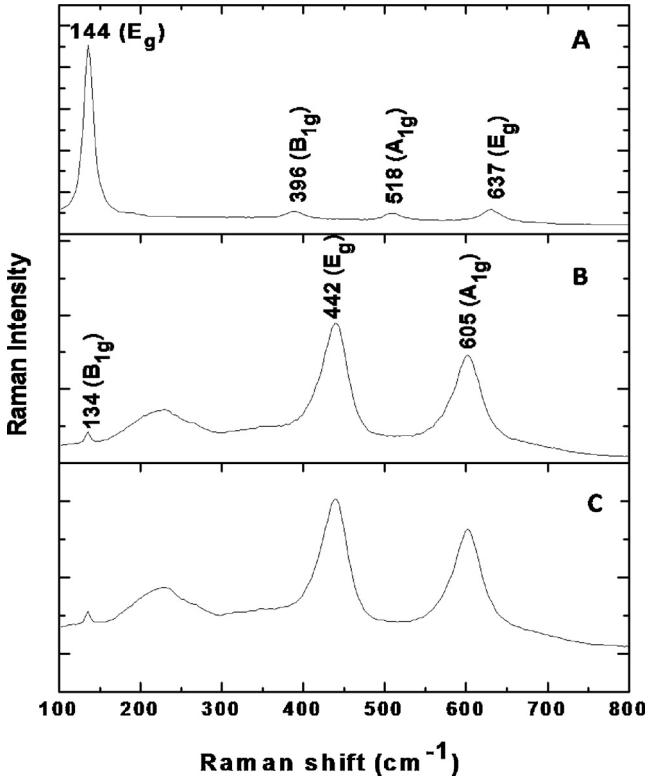

Fig. 2. Raman spectra of (A) TiO_2-500, (B) TiO_2-750 and (C) TiO_2-950 showing characteristic bands for anatase (A) and rutile (B and C).

and 49%, respectively. The collected fiber mat was left in open air to allow for complete hydrolysis of the titanium propoxide by moisture in the air [28]. The electrospun PVP/TP composite nanofibers were calcined at temperatures of 500, 750 and 950 °C for 3 h under air, removing PVP which acts as a sacrificial polymer to obtain purely inorganic TiO_2 nanofibers (labelled as TiO_2-500, TiO_2-750 and TiO_2-950, respectively).

2.3. Decoration of TiO_2 fibers

2.3.1. Phthalocyanine-decorated fibers

The deposition of complex **1** on the surfaces of each of the calcined TiO_2 fibers (TiO_2-500, TiO_2-750 and TiO_2-950) and on commercially available P25-TiO_2 (used as reference) was conducted. Complex **1** (10 mg) was dissolved in 15 mL tetrahydrofuran (THF) in four separate reaction vessels followed by immersion of TiO_2-500, TiO_2-750, TiO_2-950 or P25-TiO_2 (50 mg) into each Pc solution. The solutions were then sealed and left in the dark for 24 h at room temperature. The fibers were then removed from the solutions, rinsed with THF and oven dried at 70 °C for an hour to remove the THF. The TiO_2 based catalysts obtained were blue and are labeled TiO_2-500-**1**, TiO_2-750-**1**, TiO_2-950-**1** and P25-TiO_2-**1**.

2.3.2. Pd-decorated fibers

PdNPs were synthesized by reduction of Pd^{2+} under UVA irradiation in the presence of the calcined TiO_2 fibers (TiO_2-500, TiO_2-750 or TiO2-950) or P25-TiO_2. This was done following the protocols previously described [31] with slight modifications. Each of the calcined fibers and P25-TiO_2 (500 mg) together with $PdCl_2$ (22 mg) were added to 20 mL water in separate reaction vessels followed by UVA irradiation in a photoreactor for 8 h. The fibers were then rinsed with water and dried overnight in a desiccator. Brown Pd decorated TiO_2 based catalysts were obtained and denoted TiO_2-500-**Pd**, TiO_2-750-**Pd**, TiO_2-950-**Pd** and P25-TiO_2-**Pd**.

2.3.3. Co-decorated fibers

The Co-decorated TiO_2 catalysts were also obtained following the protocols previously described [32] with slight modifications. Irgacure-907 (I-907) was used as a photoinitiator for the photochemical reduction of Co^{2+} to CoNPs. Each of the calcined fibers and P25-TiO_2 (160 mg) were added to a 20 mL solution of 1 mM cobalt nitrate and 2 mM I-907 in argon-saturated acetonitrile, followed by irradiation in a photoreactor for 2 h. The fibers were then rinsed with water and left to dry overnight. Due to the instability of the CoNPs in the presence of oxygen, the otherwise black and paramagnetic CoNPs do not exhibit paramagnetic behaviour in the presence of air and resulted in grey/white Co decorated TiO_2 based catalysts which were denoted TiO_2-500-**Co**, TiO_2-750-**Co**, TiO_2-950-**Co** and P25-TiO_2-**Co**, respectively.

2.4. Photo-induced hydrogen generation

Each of the functionalised fibers (10 mg) were suspended in 4 mL of 1% methanol aqueous solution under argon atmosphere and sealed in a crimp top vial followed by irradiation for 4 h. For comparison, the photoactivity of commercially available P25-TiO_2 was studied under the same conditions. Samples of the headspace gas were then taken with a sample lock syringe and injected in the GC-TCD wherein the H_2 signal was detected at ~ 4.0 min. The quantification of H_2 was performed using the already reported calibration curve of the gas detection in the GC-TCD instrument in the group [14].

3. Results and discussion

3.1. Characterization of TiO_2 fibers

The titania fibers were characterised using Raman, XPS, and DR spectroscopies, XRD and TEM. The Raman spectra are shown in Fig. 2. TiO_2-500 was found to have active vibrations in Raman spectroscopy located at 144 cm^{-1} (E_g), 396 cm^{-1} (B_{1g}), 518 cm^{-1} (A_{1g}) and 637 cm^{-1} (E_g) while for TiO_2-750 and TiO_2-950, vibrations at 134 cm^{-1} (B_{1g}), 236 cm^{-1} (broad band), 442 cm^{-1} (E_g), and 605 cm^{-1} (A_{1g}) were observed, corresponding to reported vibrations for anatase and rutile crystalline phases of TiO_2 [33]. The results suggest that TiO_2-500 is pure anatase while TiO_2-750 and TiO_2-950 are pure rutile.

XRD analyses were also conducted to confirm the crystalline structure of the TiO_2 fibers. XRD patterns of the calcined fibers are shown in Fig. 3 where strong diffraction lines are observed, each of which showing high crystallinity and single phases of the TiO_2 fibers. The peak positions of TiO_2-750 and TiO_2-950 are the same suggesting

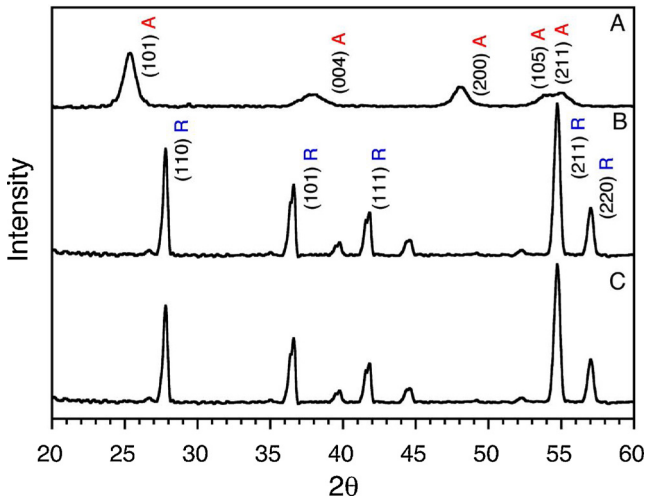

Fig. 3. XRD patterns of (A) TiO_2-500, (B) TiO_2-750 and (C) TiO_2-950; A = anatase and R = rutile.

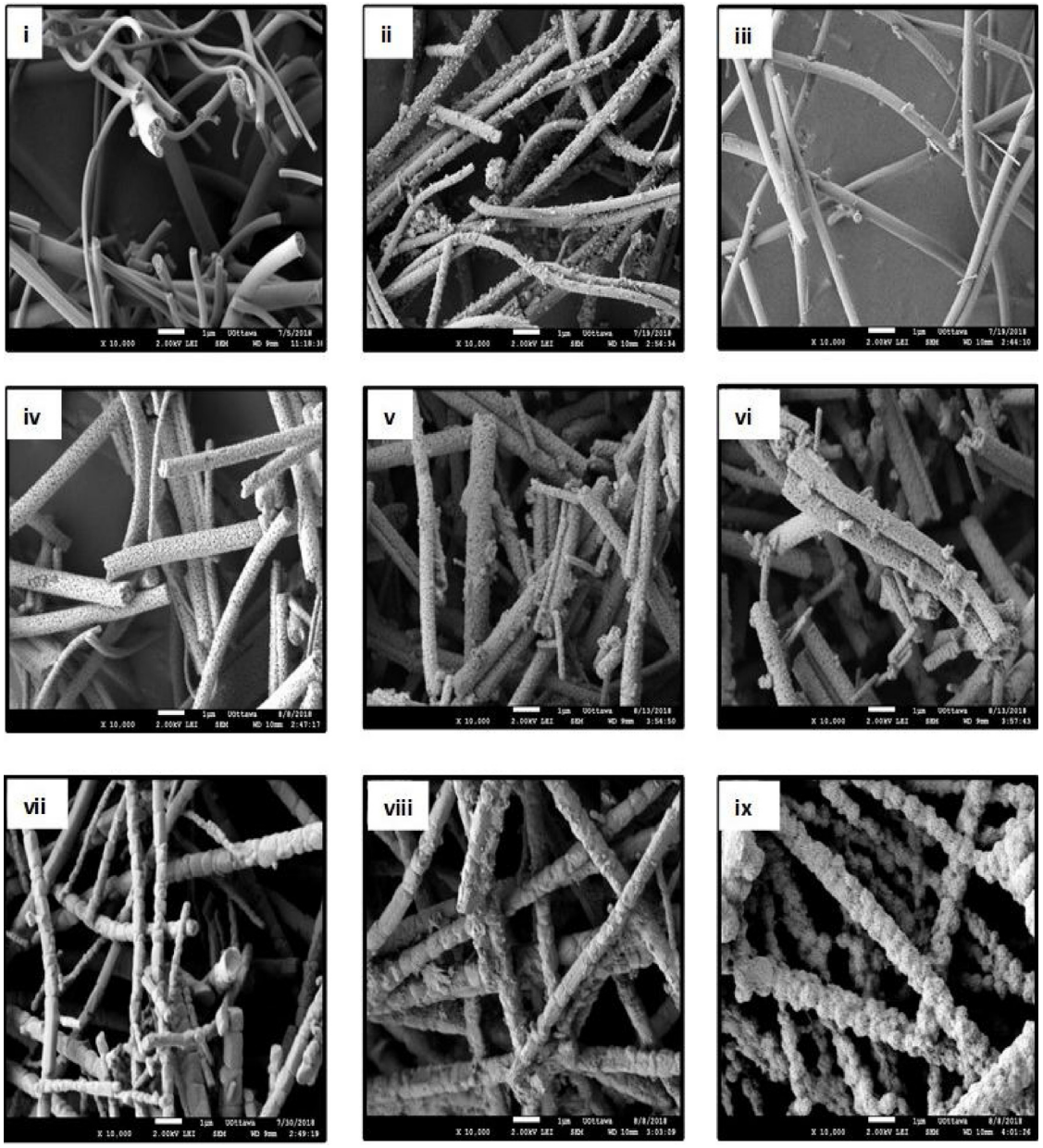

Fig. 4. SEM images of (i) TiO_2-500, (ii) TiO_2-500-**Pd**, (iii) TiO_2-500-**Co**, (iv) TiO_2-750, (v)TiO_2-750-**Pd** (vi) TiO_2-750-**Co**, (vii) TiO_2-950 (viii) TiO_2-950-**Pd** (ix) TiO_2-950-**Co.** The size bar (bottom center of each image) is 1 μm.

that they have the same phase while those of TiO_2-500 are different. For TiO_2-500, peaks were observed at the 2θ values of 25.37, 37.89, 48.02, 54.07, and 55.20 corresponding to the (101), (004), (200), (105) and (211) planes of tetragonal anatase phase as reported before [8]. For TiO_2-750 and TiO_2-950 on the other hand, the main peaks were observed at 2θ values of 27.90, 36.63, 41.83, 54.63 and 57.03° corresponding to the (110), (101), (111), (211) and (220) planes of tetragonal rutile phase as reported before [8].

The MNP- and Pc-decorated fibers were characterized by UV–vis spectroscopy. The spectrum of complex **1** in THF is shown in Fig. **S2** where the two major absorption bands associated with Pcs, i.e., the Q band (accompanied by two vibronic bands) in the near infrared region (~680 nm) and a weaker B band towards the ultraviolet region were observed. The narrow Q band of the Pc at 680 nm served as confirmation of its monomeric behaviour in THF. Solid state spectroscopy of the fibers was also conducted as shown in Fig. **S3** (using TiO_2-500, TiO_2-500-**1**, TiO_2-500-**Pd** and TiO_2-500-**Co** as examples). The diffuse reflectance spectra of the calcined TiO_2 fibers show a broad peak in the UV region (< 400) which is characteristic for TiO_2 materials [34]. The peak attributed to TiO_2 was maintained after deposition of the Pd and Co NPs as well as complex **1** on the surface of the TiO_2 fibers. The fibers decorated with the PdNPs exhibit a slight red shift and broadening in the spectral band which is not observed for the fibers decorated with the Co nanoparticles. In addition, there is also an observed red shift of the Pc Q band (692 nm) for the fibers decorated with complex **1**. The red shift and broadening of the Q band are typical of Pcs in the solid state, mainly due to aggregation, which is judged by broadening and splitting of the Pc Q band [35,36]. The inset in Fig. **S3** shows the macroscopic appearance of the materials, clearly fibers retain their paper-like fibrous morphology upon the post-synthetic decoration and change from white to gray or green color accordingly. Similar spectra were obtained for TiO_2-750 and TiO_2-950 as well as their decorated counterparts.

Analysis of the metal loading on each of the calcined fibers was

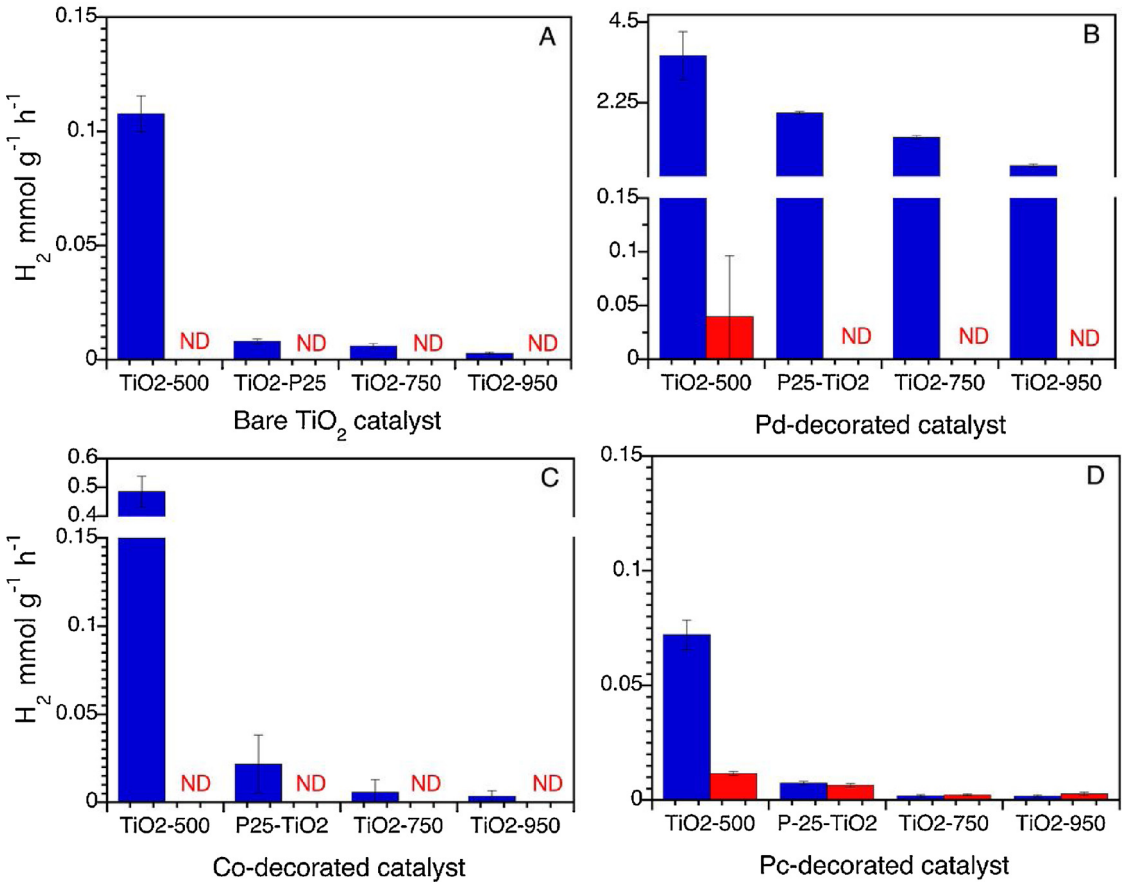

Fig. 5. H_2 generation rates with (A) bare fibers, (B) fibers decorated with Pd NPs, (C) fibers decorated with Co NPs and (D) fibers decorated with complex **1**. Tests were conducted using an irradiance of 16 W m^{-2} at 368 nm (blue) and 630 nm (red) in the presence of 1% methanol. ND: not detected.

conducted using ICP-OES and the results obtained are shown in Table S**1**. It is important to note that the Pd loadings on the three fibers (TiO_2-500-**Pd** > TiO_2-750-**Pd** ~ TiO_2-950-**Pd**) are different. This is related to the preparation method of the Pd-decorated fibers. This method uses the reducing properties of TiO_2 to reduce Pd^{2+} into Pd^0, thus the fibers catalyse the photoreduction process. TiO_2-500-**Pd** has a greater Pd loading (~3.26 wt %), presumably as a result of a higher photoreduction efficiency of TiO_2-500, while TiO_2-750-**Pd** and TiO_2-950-**Pd** have comparable loadings (~1.3 wt %). This is not surprising as the pore volume (BET, see below) of TiO_2-500 is larger (0.167 cm^3/g) than that of TiO_2-750 (0.013 cm^3/g) and increased porosity has been reported to increase the catalytic activity [15]. In addition, anatase phase TiO_2 has been reported to possess better photocatalytic activity than rutile [24]. In the case of Co decoration, same loadings are found, as I-907 was used as reducing agent. In the case of the Pc decorated fibers, no activity of the fibers is used for derivatization, they are dyed in the same manner hence the loading is also the same. Notice that the loading for the Pc-decorated fibers was determined based on the presence of Zn (central metal of the Pc).

Confirmation of efficient photoreduction of Pd^{2+} and Co^{2+} to form the nanoparticles on the surface of the bare fibers was conducted by XPS using TiO_2-500-**Pd** and TiO_2-500-**Co** as examples. A Pd 3d core level spectrum consisting of two components i.e., Pd $3d_{5/2}$ and Pd $3d_{3/2}$ (separated by approximately 5.4 eV) was obtained as reported before [37]. As shown in Fig. S**4A**, the Pd 3d spectrum of TiO_2-500-**Pd** was deconvoluted to four peaks at 336.9 (Pd^0), 337.7 (Pd^{2+}), 342.3 (Pd^0) and 343.9 eV (Pd^{2+}). The Pd^0 peaks are of higher intensity than those of Pd^{2+} which could be an indication that although there are still traces of Pd^{2+} in the fibers, the nanoparticles in the form of Pd^0 are dominant. For the CoNPs, the Co 2p core level spectrum was performed by using two spin-orbit split components i.e., Co $2p_{3/2}$ and Co $2p_{1/2}$ (separated by 15.5 eV) as observed before [38]. As shown in Fig. S**4B**, the Co 2p spectrum of TiO_2-500-**Co** was deconvoluted to two peaks at 778.1 (Co^0) and 793.6 eV (Co^0). To our surprise, given the easy oxidation of Co, the results support the complete reduction of Co^{2+} to Co^0.

Analyses of the topography of the calcined fibers before and after deposition of the MNPs were conducted using SEM (Fig. 4). Some of the calcined fibers are visibly porous; this is a good attribute relative to the commercially available P25-TiO_2 (image not shown) as it has been reported that porous nanostructured materials are more efficient photocatalyst [15]. This is due to their better mass transport, large specific surface area and abundant active sites for the reactions [39]. TiO_2-750 and TiO_2-950 have both been proven to be rutile (XRD and Raman spectra), they however possess different morphologies. The TiO_2-750 fibers are more cylindrical and porous while TiO_2-950 has a more distorted surface with grain-like structures which are sintered. The distortion of the fibers with increased calcination temperature is possibly due to the breakage of the Ti–O bonds in the anatase structure, permitting the rearrangement of Ti–O to form the thermodynamically stable rutile phase. Thus, phase transformation can lead to the disruption of the lattice of TiO_2 [40]. There are no notable differences in the images of fibers decorated with complex **1** because of the small sizes of the Pcs (about 1 nm) hence their images are not shown. The decoration of the fibers with the Pd and Co NPs on the other hand is visible on the images as the surfaces of the fibers appear rough due to the presence of the NPs.

Since some of the fibers are visibly porous (Fig. 4), the analyses of their surface areas and porosity was conducted, Table S1. No BET isotherm and hence no surface area/porosity data was obtained upon analysis of the bare and decorated TiO_2-950 fibers, this is probably due

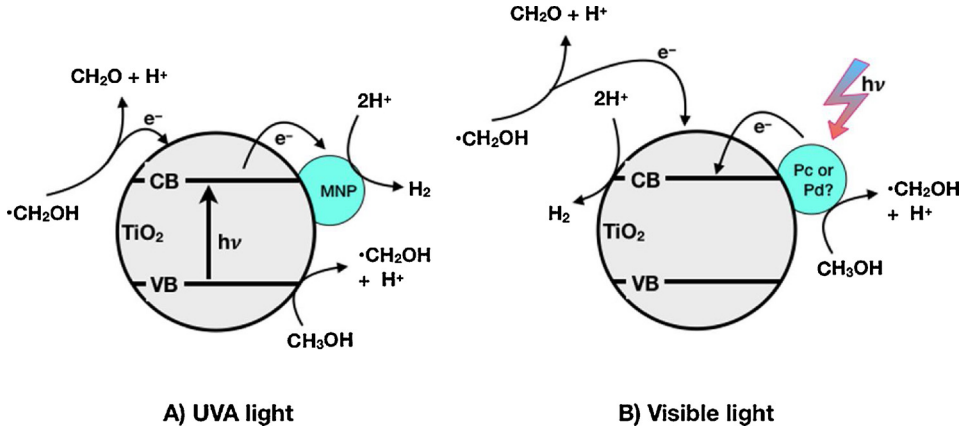

Scheme 2. Mechanism of photoactivity of the decorated TiO_2 fibers under UVA (A) and visible (B) irradiation and in the presence of methanol as SED. Note that the $^{\bullet}CH_2OH$ radical can donate an electron to the CB and contribute to hydrogen generation.

to their brittle nature and distorted fibers. Analyses of the bare TiO_2-500 and TiO_2-750 fibers shows that increased heating temperature caused a decrease in the surface area and pore volume of the fibers. Decoration of the bare fibers with NPs resulted in an increased surface area for TiO_2-500-**Pd** (or **Co**) and TiO_2-750-**Pd** (or **Co**), the former being larger than the latter. Decoration of the fibers with complex **1** only slightly affected the fibers surface area and porosity, attributed to the small size and low loadings of **1**. A significant decrease in pore volume and increase in surface area was also observed for TiO_2-500-**Pd** and TiO_2-750-**Pd**, possibly because the PdNPs fill and clog the fiber pores with that pattern not being observed for the Co decorated fibers.

3.2. Photo-induced hydrogen generation

The generation of H_2 was evaluated for each of the functionalized fibers and, for comparison, P25-TiO_2 in the presence of 1% of methanol. H_2 generation from the bare fibers (Fig. 5A) showed that the pure anatase fibers (TiO_2-500) have better photoactivity compared to rutile counterparts, as previously suggested [40]. The high activity of anatase relative to rutile has also been ascribed to it having slower charge recombination kinetics than rutile [41,42]. Indeed, P25-TiO_2 (comprised by > 70% anatase and small amounts of rutile and amorphous phase [43,44]) shows poorer activity comparing to TiO_2-500, but better activity than TiO_2-750 and TiO_2-950 (pure rutile). The bare fibers showed no activity at 630 nm, which was expected as TiO_2 does not absorb visible light [45]. The use of selected LED wavelengths (368 and 630 nm) facilitates the distinction of effects resulting from TiO_2 excitation and those due to excitation of decorating materials.

Using Co-decorated fibers under UV light excitation (Fig. 5C), the H_2 generation was enhanced ~5 times comparing to the bare fibers, similar to our observations with powder nanometric TiO_2. More interestingly, Pd-decorated fibers showed a 35-fold increase in activity (Fig. 5B). This correlates to what has been observed before where PdNPs were found to be good at enhancing SED assisted H_2 generation while CoNPs enhance true water splitting (in the absence of a SED) [14]. Decoration of the fibers with complex **1** showed a decrease in H_2 generation using UV excitation. Thus, although a zinc Pc has been reported to be effective in H_2 generation [15], our results showed lower H_2 generation for catalysts decorated with complex **1** relative to the bare TiO_2 fibers under UV irradiation. However, under visible light irradiation the Pc-decorated fibers with the best reproducible H_2 generation ability is the anatase TiO_2-500-**1**. There are some indications that TiO_2-500-Pd may also generate some H_2, but the results were not reproducible to claim that this material is a reliable H_2 source with visible light (note error bars in Fig. 5B).

From results reported here, it is clear that regeneratable electrospun titania fibers are good catalysts for metal reduction (as shown in the catalyst synthesis) as well as H_2 generation in the presence of organic compounds, a characteristic that is attractive for water purification strategies in flow systems.

3.3. Mechanism of photocatalysis

Based on the above experimental results, a possible mechanism of H_2 evolution using the decorated fibers is proposed and shown in Scheme 2.

Under UV light excitation, the photogenerated electrons in the TiO_2 conduction band are trapped by Pd or Co, delaying the electron-hole recombination process and thus favouring H_2 production Scheme 2A. In the case of the fibers decorated with a Pc (complex **1**), the Pc has a dual role wherein it acts as a sensitizer donates electrons to TiO_2 following the absorption of visible light and leaving behind photogenerated vacancies in the highest occupied molecular orbital (HOMO). This characteristic is reminiscent of Au@CeO_2 that generates H_2 with EDTA as SED [46]. Thus excited dye and possibly PdNP inject electrons into the conduction band of the TiO_2 thus enabling hydrogen formation. In all our examples, methanol acts as a sacrificial electron donor forming formaldehyde as part of the same process. Given the exceptional electrophilic properties of the TiO_2 hole [14] we anticipate that many molecules that are present in water streams as contaminants will be degraded by processes similar to that in Scheme 2 where methanol acts as a surrogate contaminant.

4. Conclusion

The work reported here shows that decorated TiO_2 fibers are excellent catalysts for SED decomposition and hydrogen generation. In our case we have used methanol as a convenient SED in order to test catalyst performance, but our earlier work shows that similar reactivity can be observed with many other organic substrates –including some, such as acetonitrile, that can hardly be regarded as typical SEDs [16]. Thus, we expect these materials to perform well for water remediation applications where typical contaminants may include household pollutants and pharmaceuticals. In contrast to typical powder titania catalysts, the materials prepared here (see Fig. 1) are robust paper-like catalysts that can be easily manipulated. They can be readily cut with scissors into any desirable shape, and even in our small-scale production, the initial bare samples were the size of a conventional letter size page. In summary, not only are the new catalysts excellent for the decomposition of organic matter and the production of hydrogen, they are also robust, easy to shape into desired macroscopic morphology and hold promise for flow applications.

Declaration of Competing Interest

There are no conflicts to declare.

Acknowledgements

This work was supported by the African Laser Centre (ALC), the Department of Science and Technology (DST), CSIR National Laser Centre, Rental Pool Programme, National Research Foundation (NRF) of South Africa through DST/NRF South African Research Chairs Initiative for Professor of Medicinal Chemistry and Nanotechnology (UID 62620), Rhodes University, the Natural Sciences and Engineering Research Council of Canada, the Canada Foundation for Innovation, the Canada Research Chairs Program and Canada's International Development Research Centre (IDRC).

Appendix A. Supplementary data

Supplementary material related to this article can be found, in the online version, at doi:https://doi.org/10.1016/j.jphotochem.2019.112185.

References

[1] D.F. Ollis, C. Turchi, Heterogeneous photocatalysis for water-purification - contaminant mineralization kinetics and elementary reactor analysis, Environ. Prog. 9 (1990) 229–234.
[2] Progress on Drinking Water, Sanitation and Hygiene, 2017 Update and SDG Baselines, World Health Organization (WHO); United Nations Children's Fund (UNICEF), 2017.
[3] S.Y. Tee, K.Y. Win, W.S. Teo, L.D. Koh, S.H. Liu, C.P. Teng, M.Y. Han, Recent progress in energy-driven water splitting, Adv. Sci. 4 (2017) 1600337.
[4] A. Fujishima, K. Honda, Electrochemical photolysis of water at a semiconductor electrode, Nature 238 (1972) 37.
[5] K. Nakata, A. Fujishima, TiO_2 photocatalysis: design and applications, J. Photochem. Photobiology C-Photochem. Rev. 13 (2012) 169–189.
[6] J. Schneider, M. Matsuoka, M. Takeuchi, J. Zhang, Y. Horiuchi, M. Anpo, D.W. Bahnemann, Understanding TiO_2 photocatalysis: mechanisms and materials, Chem. Rev. 114 (2014) 9919–9986.
[7] A. Ali-Elhage, J.C. Scaiano, A.E. Lanterna, Dressing up for the occasion: the many faces of decorated titanium dioxide in photocatalysis, in: J. Pérez-Prieto, M. González-Béjar (Eds.), Photoactive Inorganic Nanoparticles, Elsevier, 2019, pp. 73–99.
[8] J. Huang, T. You, Electrospun nanofibers: from rational design, fabrication to electrochemical sensing applications, in: R. Maguire (Ed.), Advances in Nanofibers, IntechOpen, 2013.
[9] D.H. Reneker, I. Chun, Nanometre diameter fibres of polymer, produced by electrospinning, Nanotechnology 7 (1996) 216–223.
[10] Y.F. Wang, L.P. Li, X.S. Huang, Q. Li, G.S. Li, New insights into fluorinated TiO_2 (brookite, anatase and rutile) nanoparticles as efficient photocatalytic redox catalysts, RSC Adv. 5 (2015) 34302–34313.
[11] R.L. Penn, J.F. Banfield, Morphology development and crystal growth in nanocrystalline aggregates under hydrothermal conditions: insights from titania, Geochim. Cosmochim. Acta 63 (1999) 1549–1557.
[12] G. Oskam, A. Nellore, R.L. Penn, P.C. Searson, The growth kinetics of TiO_2 nanoparticles from titanium(IV) alkoxide at high water/titanium ratio, J. Phys. Chem. B 107 (2003) 1734–1738.
[13] H. Pan, Principles on design and fabrication of nanomaterials as photocatalysts for water-splitting, Renewable Sustainable Energy Rev. 57 (2016) 584–601.
[14] A.S. Hainer, J.S. Hodgins, V. Sandre, M. Vallieres, A.E. Lanterna, J.C. Scaiano, Photocatalytic hydrogen generation using metal-decorated TiO_2: sacrificial donors vs true water splitting, ACS Energy Lett. 3 (2018) 542–545.
[15] A. Tiwari, N.V. Krishna, L. Giribabu, U. Pal, Hierarchical porous TiO_2 embedded unsymmetrical zinc–Phthalocyanine sensitizer for visible-light-Induced photocatalytic H_2 production, J. Phys. Chem. C 122 (2018) 495–502.
[16] A. Hainer, N. Marina, S. Rincon, P. Costa, A.E. Lanterna, J.C. Scaiano, Highly electrophilic titania hole as a versatile and efficient photochemical free radical source, JACS 141 (2019) 4531–4535.
[17] A.E. Lanterna, J.C. Scaiano, Photoinduced hydrogen fuel production and water decontamination technologies. Orthogonal strategies with a parallel future? ACS Energy Lett. 2 (2017) 1909–1910.
[18] R. Guilard, K. Kadish, K. Smith, The Porphyrin Handbook, 1 ed., Elsevier, 2003.
[19] K. Ishii, Functional singlet oxygen generators based on phthalocyanines, Coord. Chem. Rev. 256 (2012) 1556–1568.
[20] T. Oku, N. Kakuta, K. Kobayashi, A. Suzuki, K. Kikuchi, Fabrication and characterization of TiO_2-based dye-sensitized solar cells, Progress in Natural Science-Materials International 21 (2011) 122–126.
[21] A. Sindelo, O.L. Osifeko, T. Nyokong, Synthesis, photophysicochemical and photodynamic antimicrobial chemotherapy studies of indium pyridyl phthalocyanines: charge versus bridging atom, Inorg. Chim. Acta 476 (2018) 68–76.
[22] M.S. Baptista, M. Wainwright, Photodynamic antimicrobial chemotherapy (PACT) for the treatment of malaria, leishmaniasis and trypanosomiasis, Braz. J. Med. Biol. Res. 44 (2011) 1–10.
[23] M. Wainwright, Photodynamic antimicrobial chemotherapy (PACT), J. Antimicrob. Chemother. 42 (1998) 13–28.
[24] G.G. Luo, X.C. Li, J.H. Wang, Visible light-driven hydrogen evolution from aqueous solution in a noble-metal-Free system catalyzed by a cobalt phthalocyanine, ChemistrySelect 1 (2016) 425–429.
[25] M.S. Agirtas, C. Karatas, S. Ozdemir, Synthesis of some metallophthalocyanines with dimethyl 5-(phenoxy)-isophthalate substituents and evaluation of their antioxidant-antibacterial activities, Spectrochim. Acta A. 135 (2015) 20–24.
[26] L. Zhou, E.Y. Chen, W.W. Jin, Y. Wang, J.H. Zhou, S.H. Wei, Monomer zinc phthalocyanine/upconversion nanoparticle coated with hyaluronic acid crosslinked gel as NIR light-activated drug for in vitro photodynamic therapy, Dalt. Trans. 45 (2016) 15170–15179.
[27] B. Caratao, E. Carneiro, P. Sa, B. Almeida, S. Carvalho, Properties of electrospun TiO_2 nanofibers, J. Nanotechnol. 2014 (2014) 472132.
[28] D. Li, Y.N. Xia, Fabrication of titania nanofibers by electrospinning, Nano Lett. 3 (2003) 555–560.
[29] S. Ghafoor, S.Z. Hussain, S. Waseem, S.N. Arshad, Photo-reduction of heavy metal ions and photo-disinfection of pathogenic bacteria under simulated solar light using photosensitized TiO_2 nanofibers, RSC Adv. 8 (2018) 20354–20362.
[30] A.K. Alves, F.A. Berutti, F.J. Clemens, T. Graule, C.P. Bergmann, Photocatalytic activity of titania fibers obtained by electrospinning, Mater. Res. Bull. 44 (2009) 312–317.
[31] A. Elhage, A.E. Lanterna, J.C. Scaiano, Tunable photocatalytic activity of palladium-decorated TiO_2: non hydrogen -Mediated hydrogenation or isomerization of BenzylSubstituted alkenes, ACS Catal. 7 (2017) 250–255.
[32] J.C. Scaiano, K.G. Stamplecoskie, G.L. Hallett-Tapley, Photochemical Norrish type I reaction as a tool for metal nanoparticle synthesis: importance of proton coupled electron transfer, Chem. Commun. 48 (2012) 4798–4808.
[33] M. Lubas, J.J. Jasinski, M. Sitarz, L. Kurpaska, P. Podsiad, J. Jasinski, Raman spectroscopy of TiO_2 thin films formed by hybrid treatment for biomedical applications, Spectrochim. Acta A. 133 (2014) 867–871.
[34] K. Zhou, Y. Zhu, X. Yang, X. Jiang, C. Li, Preparation of graphene–TiO_2 composites with enhanced photocatalytic activity, New J. Chem. 35 (2011) 353–359.
[35] L. Alagna, A. Capobianchi, M.P. Casaletto, G. Mattogno, A.M. Paoletti, G. Pennesi, G. Rossi, Effect of molecular packing on the solid state spectra of ruthenium phthalocyanine: anomalous behaviour of a monodimensional stacked assembly, J. Mater. Chem. 11 (2001) 1928–1935.
[36] A. Auger, P.M. Burnham, I. Chambrier, M.J. Cook, D.L. Hughes, X-Ray crystallographic studies of three substituted indium(iii) phthalocyanines: effect of ring substitution and the axial ligand on molecular geometry and packing, J. Mater. Chem. 15 (2005) 168–176.
[37] E.F. Smith, I.J. Villar Garcia, D. Briggs, P. Licence, Ionic liquids in vacuo; solution-phase X-ray photoelectron spectroscopy, Chem. Commun. (2005) 5633–5635.
[38] P. Bazylewski, D.W. Boukhvalov, A.I. Kukharenko, E.Z. Kurmaev, A. Hunt, A. Moewes, Y.H. Lee, S.O. Cholakh, G.S. Chang, The characterization of Co-nanoparticles supported on graphene, RSC Adv. 5 (2015) 75600–75606.
[39] Y. Li, Z.Y. Fu, B.L. Su, Hierarchically structured porous materials for energy conversion and storage, Adv. Funct. Mater. 22 (2012) 4634–4667.
[40] S. Madhugiri, B. Sun, P.G. Smirniotis, J.P. Ferraris, K.J. Balkus, Electrospun mesoporous titanium dioxide fibers, Microporous Mesoporous Mater. 69 (2004) 77–83.
[41] A. Fujishima, X.T. Zhang, D.A. Tryk, TiO_2 photocatalysis and related surface phenomena, Surf. Sci. Rep. 63 (2008) 515–582.
[42] A. Yamakata, T. Ishibashi, H. Onishi, Time-resolved infrared absorption study of nine TiO_2 photocatalysts, Chem. Phys. 339 (2007) 133–137.
[43] D.C. Hurum, A.G. Agrios, K.A. Gray, T. Rajh, M.C. Thurnauer, Explaining the enhanced photocatalytic activity of Degussa P25 mixed-phase TiO_2 using EPR, J. Phys. Chem. B 107 (2003) 4545–4549.
[44] B. Ohtani, O.O. Prieto-Mahaney, D. Li, R. Abe, What is Degussa (Evonik) P25? Crystalline composition analysis, reconstruction from isolated pure particles and photocatalytic activity test, J. Photochem. Photobiol. A: Chem. 216 (2010) 179–182.
[45] S.P. Pitre, T.P. Yoon, J.C. Scaiano, Titanium dioxide visible light photocatalysis: surface association enables photocatalysis with visible light irradiation, Chem. Commun. 53 (2017) 4335–4338.
[46] A. Primo, T. Marino, A. Corma, R. Molinari, H. García, Efficient visible-light photocatalytic water splitting by minute amounts of gold supported on nanoparticulate CeO_2 obtained by a biopolymer templating method, JACS 133 (2011) 6930–6933.